Available online at www.sciencedirect.com
SCIENCE DIRECT®
International Journal of Heat and Mass Transfer 47 (2004) 2849–2860
International Journal of HEAT and MASS TRANSFER
www.elsevier.com/locate/ijhmt

Laminar free convection underneath a downward facing hot fin array

A. Dayan *, R. Kushnir, G. Mittelman, A. Ullmann

Department of Fluid Mechanics and Heat transfer, Faculty of Engineering, Tel Aviv University, Ramat Aviv, 69978 Tel Aviv, Israel

Received 2 January 2003

Abstract

A combined analytical, numerical and experimental study was conducted to investigate the problem of natural convection underneath a horizontal rectangular hot fin array. This subject has not been explored before. The purpose of the investigation was to provide useful and reliable heat transfer coefficients. In addition to the experimental and numerical results, a useful approximate closed form analytical solution is offered. The analytical solution clearly reveals the dependence of the Nusselt number on the Rayleigh number, the Prandtl number and the fin's height to spacing ratio. Optimum analyses were conducted to determine the minimum fin height that provides the necessary cooling capability of a specified array base area. In this context it is shown that the optimal fin spacing varies within a narrow range which depends primarily on the array length. Those findings have important industrial application because they impact both the cost and size of cooling finned surfaces.

1. Introduction

An investigation of the problem of free convection underneath a hot and isothermal horizontal fin array is presented. A downward facing fin array is not the preferred orientation for effective cooling by means of natural convection. Thus, this problem has been neglected in the past. However, the development of modern telecommunication equipment changed this fact. Architectural design requirements give preference specifically to such hidden cooling devices. The current research effort was undertaken to provide analytical tools for calculating the cooling capabilities of downward facing rectangular fin arrays.

An extensive literature survey did not unveil any work on the subject of free convection underneath a horizontal fin array. As opposed to that, considerable literature exists on the problem of free convection underneath hot isothermal flat strips. The latter, however, exhibits convective heat transfer characteristics that apply to finned cooling surfaces as well. It has been demonstrated that buoyancy forces induce a flow from the center of the hot surface toward the edges [1,2]. Furthermore, in a practical sense, the flow near the surface exhibits some boundary layer characteristics [3]. The ambient airflow rises from below upward and towards the surface center. At a certain distance δ from the surface the airflow reverses its lateral movement direction and flows towards the surface edges, as indicated in Fig. 1. The points of flow reversal form a virtual surface that represents a boundary where the flow lacks any lateral velocity component. The flow confined between this boundary and the hot surface moves towards the surface edges while portraying some boundary layer characteristics. This layer is thickest at the surface center and thinnest at the edges. Similarly, a thermal boundary layer is also formed, as shown in Fig. 1. Both profiles exhibit self-similar characteristics along most of the strip width (excluding slight deviations at the strip edges [3]).

Practically all the heat transfer correlations for natural convection underneath hot flat strips for laminar flow, see [3] (which contains a large number of references), have the form of

$$\overline{Nu}_L^{s} = C Ra_L^{1/5} \tag{1}$$

* Corresponding author. Tel.: +972-3-640-8443; fax: +972-3-640-7334.
E-mail address: dayan@eng.tau.ac.il (A. Dayan).

0017-9310/$ - see front matter © 2004 Elsevier Ltd. All rights reserved.
doi:10.1016/j.ijheatmasstransfer.2004.01.003

Nomenclature

a	half the space between fins
A_b	array base area
A_t	array total area
c	ratio of substituted fin height to boundary layer thickness, δ_1/δ
C	coefficient, Eq. (1)
C_1, C_2	coefficients, Eq. (12)
f_i	$i = 1 \ldots 10$, Eqs. (6), (10) and (15)
f_{ii}	$i = 1 \ldots 3$, Eq. (9)
g	gravitational acceleration
$h_{y,x}$	local heat transfer coefficient at the channel base
$h_{y,z}$	fin surface local heat transfer coefficient
$\bar{h}$	average heat transfer coefficient
H	fin height
k	thermal conductivity
L	array half length
L^*	dimensionless length, $L/\sqrt[3]{\alpha v/g}$
$\dot{M}$	mass discharge rate
$\overline{Nu}_L$	average Nusselt number, $\bar{h}L/k$
P	pressure
Pr	Prandtl number, v/α
Q	heat transfer rate
Ra_L	Rayleigh number, $g\beta L^3\theta_w/\alpha v$
t	half the fin thickness
T	temperature
$\mathbf{u}$	specific internal energy
$\dot{U}$	specific internal energy flux
v_{max}	maximum velocity within the channel at location y
v^*	dimensionless velocity, v/v_{max}
u, v, w	velocity components
x, y, z	cartesian coordinate axes

Greek symbols

α	thermal diffusivity
β	thermal expansion coefficient
Γ	gamma function
δ	boundary layer depth
δ_C	critical depth at the channel edge
δ_1	substituted fin height
ε	emissivity
η	dimensionless coordinate, z/δ
ξ	dimensionless coordinate, x/a
v	kinematic viscosity
θ^*	dimensionless temperature, θ/θ_w
θ	temperature difference $(T - T_\infty)$
ρ	density

Subscripts

w	wall conditions
∞	ambient conditions
ref	reference value

Superscript

s	flat strip

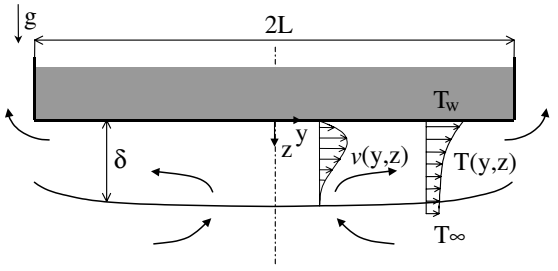

Fig. 1. Schematic description of natural convection underneath a hot horizontal flat strip.

where $\overline{Nu}_L^s$ is the averaged Nusselt number, Ra_L the Rayleigh number, and C is a coefficient that depends on the surface geometry and Prandtl number. The relevance of these correlations, for the present study, stems from the fact that they apply for the limiting cases of arrays with large or small fin spacing. In this respect, Aihara et al. [1] investigated experimentally a two-dimensional airflow underneath a rectangular plate. Their investigation revealed that it is reasonable to define a boundary layer zone with characteristic temperature and velocity profiles that suit well integral method analyses.

The current work was initiated by conducting an in depth investigation of the horizontal flat-strip case. During that research phase, the integral method was applied to develop a closed form solution [3] for the Nusselt number. Additionally, it unveiled the reason for the discrepancy that exists amongst the corresponding correlations found in the literature. In essence, the discrepancy emanate from the relative importance of edge effects. The new correlation that was developed for $Pr = 0.7$ is

$$\overline{Nu}_L^s = [1 + 0.24\exp(-0.0025L^*)]0.46Ra_L^{1/5} \quad (2)$$

where

$$L^* = \frac{L}{\sqrt[3]{\alpha v/g}}$$

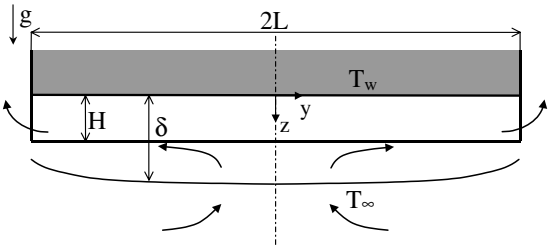

Fig. 2. Schematic description of natural convection underneath a hot finned surface.

The dimensionless length L^* contains a group of properties that affect the boundary layer thickness which increases with the thermal diffusivity α and kinematic viscosity ν, and decreases with the gravitational acceleration g. The influence of this dimensionless parameter is pronounced when the strip width is short and "edge effects" are no longer negligible.

Similar to the flow near a flat surface, a "boundary layer" type flow is expected to develop underneath a finned surface, as shown in Fig. 2. Qualitative visualization tests, conducted with smoke, and numerical simulations supported that fact. However, a finned surface has the added dimensions of the fins geometry. The shape of the "boundary layer" outer surface is affected by the presence of the fins. A fin array can be regarded as an array of inverted channels. The "boundary layer" outer surface, excluding the surface edges neighborhood, can be either entirely outside or partially outside those channels. The former case, shown in Fig. 2, is the focus of the current investigation. It covers all the cases of practical importance where the fin spacing is not much larger than its optimum (presented subsequently in this work). For those cases, the "boundary layer" outer surface is laterally fairly flat and slightly curved longitudinally.

The current work was undertaken with the purpose of providing reliable heat transfer coefficients of downward facing rectangular fin arrays. The investigation was conducted experimentally, numerically and analytically. The numerical simulation was tested experimentally and then used to extend the scope of the experimental data. The numerical analyses were conducted over a large range of Rayleigh numbers and array dimensions. The analytical phase of the research was aimed towards the development of a useful closed form expression for *Nu* number. In addition, optimization analyses were conducted to find the fin array dimensions that maximize the cooling capability per unit base area for a given fin height. It is worth noting that the analytical approach that was used here and previously [3] can be considered as a simple and attractive solution method that can be incorporated for the analyses of even more complex hot surface geometry.

2. Analytical solution

Consider a horizontal isothermal hot rectangular fin array. Excluding side effects, it is expected that the hydrodynamic and thermal conditions within all the fin array channels would be identical. Therefore it suffices to model the conditions of a single channel. As seen in Fig. 3a, the channel is of length $2L$, in between two fins of height H that are $2a$ apart. The fin thickness $2t$ is usually small relative to the channel circumference and therefore its influence on the average heat transfer coefficient is insignificant. Therefore, that influence would not be analyzed specifically. The cooling effect of the fin-edges exposed area would be accounted for simply as an added area. As aforementioned, it is assumed that the boundary layer thickness extends beyond the fin height along most of the channel length. If one wants to adopt the integral solution method for that boundary layer, the rectangular fin geometry poses a serious obstacle. Its fixed height contradicts the similarity characteristics of boundary layer velocity and temperature profiles. In other words, if the boundary layer outer surface curves longitudinally and shrinks as it approaches the cannel edge, the fixed fin height would distort it. Luckily, the domain where this effect plays a role is confined to a relatively short section near the channel edge. Throughout the cannel length, such as underneath flat surfaces [3], the boundary layer thickness is fairly constant (as observed in the numerical simulation). Thus the question that arises is what a difference it could make if the fin geometry is distorted such that the fin height would be proportional to the boundary layer thickness. If the boundary layer thickness was constant then that assumption would be fully accurate. The argument that is introduced here is, in effect, that a slightly curved fin should have a similar cooling capability such as a rectangular fin of equal surface area. The merit of this assumption, that has been indeed adopted, is twofold, first, it entails a substantial simplification of the analytical model, and second, it does not affect much the model accuracy (as seen subsequently).

Based on the aforementioned discussion, the height of the curved fin δ_1, shown in Fig. 3b, is considered to be

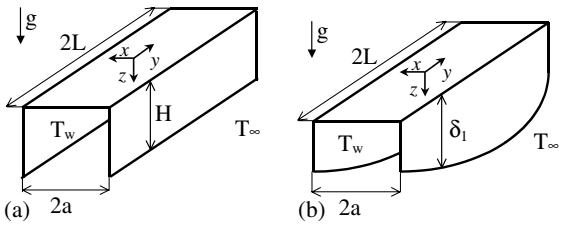

Fig. 3. Dimensions and coordinate system of a channel. (a) Rectangular fin; (b) curved fin.

directly proportional to the boundary layer thickness δ by a constant factor c (i.e. $\delta_1 = c\delta$, $c \leqslant 1$). For the indicated coordinate system, the continuity, momentum and energy equations subject to, both, the boundary layer and the Bousinesq approximations are

$$\frac{\partial u}{\partial x} + \frac{\partial v}{\partial y} + \frac{\partial w}{\partial z} = 0 \tag{3a}$$

$$\frac{\partial p}{\partial x} = 0 \tag{3b}$$

$$u\frac{\partial v}{\partial x} + v\frac{\partial v}{\partial y} + w\frac{\partial v}{\partial z} = -\frac{1}{\rho_\infty}\frac{\partial p}{\partial y} + \nu\left(\frac{\partial^2 v}{\partial x^2} + \frac{\partial^2 v}{\partial z^2}\right) \tag{3c}$$

$$\rho_\infty(1-\beta\theta)g - \frac{\partial p}{\partial z} = 0 \tag{3d}$$

and

$$u\frac{\partial \theta}{\partial x} + v\frac{\partial \theta}{\partial y} + w\frac{\partial \theta}{\partial z} = \alpha\left(\frac{\partial^2 \theta}{\partial x^2} + \frac{\partial^2 \theta}{\partial z^2}\right) \tag{3e}$$

The boundary conditions for a constant wall temperature are

$$z = 0, \quad u = v = w = 0, \quad \theta = \theta_w \tag{4a}$$

$$x = \pm a, \quad 0 \leqslant z \leqslant \delta_1, \quad u = v = w = 0, \quad \theta = \theta_w \tag{4b}$$

$$x = \pm a, \quad \delta_1 \leqslant z \leqslant \delta, \quad u = 0, \quad \frac{\partial v}{\partial x} = 0, \quad \frac{\partial \theta}{\partial x} = 0 \tag{4c}$$

$$z = \delta, \quad u = v = 0, \quad \frac{\partial v}{\partial z} = 0, \quad \theta = 0, \quad \frac{\partial \theta}{\partial z} = 0 \tag{4d}$$

for fluids with Prandtl numbers close to unity it is reasonable to assume that the momentum and the temperature boundary layers have an identical thickness δ.

The set of governing equations can be solved by the integral solution method based on the assumption that the velocity and temperature profiles exhibit similarity characteristics. The existence of similarity profiles was examined numerically and found to be accurate for the temperature profiles, excluding at the channel edges. The velocity profiles along the channel were found self-similar in the x-direction and roughly so in the z-direction. The latter was found to be self-similar in the portion of the flow that extends from δ to δ_1. Within the channels, some deviations from similarity were observed, more in the shape and less in the wall velocity gradients. However, the existence of similarity in the temperature profiles is the dominant factor for heat transport calculations. Consequently, it was assumed that the velocity profile deviations are modest enough to be tolerated by the integral solution method.

The selected self-similar velocity and temperatures profiles have the form of

$$v^*(\eta,\xi) = \frac{v}{v_{max}} \tag{5a}$$

$$\theta^*(\eta,\xi) = \frac{\theta}{\theta_w} \tag{5b}$$

respectively, where $\eta = z/\delta$, $\xi = x/a$, and v_{max} is the maximum velocity at any channel cross section (i.e. v_{max} is y dependent only).

The substitution of the velocity and temperature profiles (5) into Eqs. (3a)–(3e) and integration across the boundary layer cross section area, subject to the boundary conditions, yields

$$f_1\frac{d(v_{max}^2\delta)}{dy} + f_2 g\beta\theta_w\delta\frac{d\delta}{dy} + \left[f_3\frac{\delta^2 c^2}{a^2} + f_4\right]\frac{\nu v_{max}}{\delta} = 0 \tag{6a}$$

$$f_5\frac{d(v_{max}\delta)}{dy} = \left[f_6\frac{\delta^2 c^2}{a^2} + f_7\right]\frac{\alpha}{\delta} \tag{6b}$$

where

$$f_1 = \int_{-1}^{1}\int_0^1 v^{*2}\,d\eta\,d\xi \quad f_2 = 2\int_{-1}^{1}\int_0^1\int_\eta^1 \theta^*\,d\eta'\,d\eta\,d\xi$$

$$f_3 = \frac{-2}{c^2}\int_0^1 \frac{\partial v^*}{\partial\xi}_{|\xi=1} d\eta \quad f_4 = \int_{-1}^{1}\frac{\partial v^*}{\partial\eta}_{|\eta=0} d\xi$$

$$f_5 = \int_{-1}^{1}\int_0^1 v^*\theta^*\,d\eta\,d\xi \quad f_6 = \frac{2}{c^2}\int_0^1 \frac{\partial\theta^*}{\partial\xi}_{|\xi=1} d\eta$$

$$f_7 = -\int_{-1}^{1}\frac{\partial\theta^*}{\partial\eta}_{|\eta=0} d\xi$$

All the coefficients, f_1 through f_7 are dependent on the velocity and temperature profiles. The boundary conditions at the channel center and at its edge are

$$\text{at } y = 0 \quad v_{max} = 0 \tag{7a}$$

$$\text{at } y = L \quad \delta = \delta_C \tag{7b}$$

where δ_C is the boundary layer thickness for critical flow conditions at the channel edge.

From all five terms of Eqs. (6a) and (6b), the buoyancy term is the only one that is notably dependent on the boundary layer shape, or alternatively to the longitudinal derivative of its thickness. The boundary layer curvature has little effects on all other terms. Based on, either, our numerical simulation or dimensional analyses, one can find that the boundary layer thickness is fairly uniform along most of the flow run. Applying these conclusions significantly simplified the solution of the equations. This approach was successfully incorporated in the flat-strip investigation [3].

For a nearly constant boundary layer thickness, the first order approximation of the energy equation solution is

$$v_{max} = \frac{f_{33}\alpha y}{\delta^2} \tag{8}$$

Substituting Eq. (8) for the momentum equation velocity terms, and retaining the boundary-layer-thickness

derivative only for the buoyancy term, yields the following first order solution approximation

$$\delta = \left[\delta_C^5 + \frac{5\alpha^2}{2f_{11}}\frac{(2f_{33}^2 + f_{22}f_{33}Pr)\cdot(L^2-y^2)}{g\beta\theta_w}\right]^{1/5} \tag{9}$$

where

$$f_{11} = \frac{f_2}{f_1} \quad f_{22} = \frac{f_3\left(\frac{H}{a}\right)^2 + f_4}{f_1} \quad f_{33} = \frac{f_6\left(\frac{H}{a}\right)^2 + f_7}{f_5}$$

The boundary layer thickness at the channel edge, δ_C, is calculated for critical flow conditions at that point. As seen from the solution, the fluid velocity increases as it approaches the channel edge, where the boundary layer assumes its minimal thickness. The critical thickness, at the edge, provides a maximal mass discharge rate for the local fluid energy [3,4]. Based on these arguments the critical boundary layer thickness was found to be (see Appendix A for the derivation details)

$$\delta_C = \left(\frac{2f_8f_{33}^2\alpha^2L^2}{f_9g\beta\theta_w}\right)^{1/5} \tag{10}$$

where

$$f_8 = \frac{1}{2}\int_{-1}^{1}\int_{0}^{1} v^{*3}\,d\eta\,d\xi$$
$$f_9 = \int_{-1}^{1}\int_{0}^{1}\left[\left(\int_{\eta}^{1}\theta^*\,d\eta'\right)v^* + \theta^*v^*\eta\right]d\eta\,d\xi$$

It is well known that in open channels the critical depth occurs at about $2\delta_C$ upstream the channel edge [5]. It is thus common to estimate the fluid depth at the channel edge to be somewhat smaller than the theoretical critical depth. We therefore assumed that the boundary layer critical thickness at the strip edges equals $0.9\delta_C$, or

$$\begin{aligned}\delta &= \left[\frac{2f_8f_{33}^2\alpha^2L^20.9^5}{f_9g\beta\theta_w} + \frac{5}{2}\frac{\alpha^2(2f_{33}^2 + f_{22}f_{33}Pr)\cdot(L^2-y^2)}{f_{11}g\beta\theta_w}\right]^{1/5}\\ &= L\left[C_1 - C_2\left(\frac{y}{L}\right)^2\right]^{1/5}(Ra_LPr)^{-1/5}\end{aligned} \tag{11}$$

The coefficients C_1 and C_2 are

$$\begin{aligned}C_1 &= 2\times 0.9^5\frac{f_8f_{33}^2}{f_9} + \frac{5}{2}\frac{(2f_{33}^2 + f_{22}f_{33}Pr)}{f_{11}}\\ C_2 &= \frac{5}{2}\frac{(2f_{33}^2 + f_{22}f_{33}Pr)}{f_{11}}\end{aligned} \tag{12}$$

The local heat transfer coefficients, for the temperature profile (5b), are

$$h_{y,x} = -\frac{k}{\theta_w}\frac{\partial\theta}{\partial z}_{|z=0} = -\frac{k}{\delta}\frac{\partial\theta^*}{\partial\eta}_{|\eta=0} \tag{13a}$$

$$h_{y,z} = +\frac{k}{\theta_w}\frac{\partial\theta}{\partial x}_{|x=a} = +\frac{k}{a}\frac{\partial\theta^*}{\partial\xi}_{|\xi=1} \tag{13b}$$

The average heat transfer coefficient, $\bar{h}$, is therefore

$$\begin{aligned}\bar{h} &= \frac{1}{A_t}\int\int_{A_t} h\,dA\\ &= \frac{1}{L(a+H)}\left[\int_0^L\int_0^a h_{y,x}\,dx\,dy + \int_0^L\int_0^{\delta_1} h_{y,z}\,dz\,dy\right]\end{aligned} \tag{14}$$

Notice that the curved fin area is identical to that of the rectangular fin. The corresponding averaged Nusselt number is obtained from the substitution of the boundary layer thickness, Eq. (11), into Eq. (14) and is

$$\begin{aligned}\overline{Nu}_L &= \frac{\bar{h}L}{k}\\ &= \frac{1}{\left(1+\frac{H}{a}\right)}\left[\frac{f_7}{2}C_1^{-\frac{1}{5}}F\left(\frac{1}{5},\frac{1}{2};\frac{3}{2};\frac{C_2}{C_1}\right)(Ra_LPr)^{\frac{1}{5}} + \frac{f_{10}}{c}\left(\frac{H}{a}\right)\left(\frac{L}{a}\right)\right]\end{aligned} \tag{15}$$

where $F(w,x;y;z)$ is the Gauss hyper-geometric function defined by

$$F(w,x;y;z) = \frac{\Gamma(y)}{\Gamma(w)\Gamma(x)}\sum_{n=0}^{\infty}\frac{\Gamma(w+n)\Gamma(x+n)}{\Gamma(y+n)}\cdot\frac{z^n}{n!} \tag{16}$$

and

$$f_7 = -\int_{-1}^{1}\frac{\partial\theta^*}{\partial\eta}_{|\eta=0}d\xi \quad f_{10} = \int_0^c\frac{\partial\theta^*}{\partial\xi}_{|\xi=1}d\eta$$

The constant factor c is calculated from the requirement that the curved fin surface area should be equal to that of the rectangular fin, hence

$$H = \frac{1}{L}\int_0^L \delta_1\,dy \tag{17}$$

which after integration yields

$$cC_1^{\frac{1}{5}}F\left(-\frac{1}{5},\frac{1}{2};\frac{3}{2};\frac{C_2}{C_1}\right) = \left(\frac{H}{L}\right)(Ra_LPr)^{\frac{1}{5}} \tag{18}$$

Since C_1 and C_2 are functions of c, Eq. (18) is an implicit solution for c. Once c is obtained, it is substituted in Eq. (15) for the Nusselt number evaluation. Notice that, the above derivation is valid for any velocity and temperature profiles that have the forms of Eqs. (5a) and (5b), respectively.

3. Experimental apparatus

The test apparatus consisted of an insulated horizontal aluminum fin array that was electrically heated

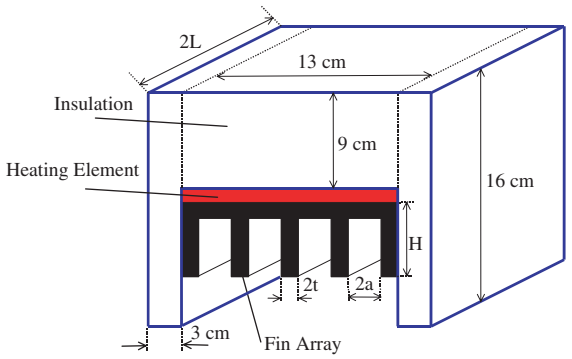

Fig. 4. Experimental setup.

on its upper surface, as shown in Fig. 4. Six different fin arrays were tested, for sensitivity analyses, the dimensions of which are listed in Table 1. The insulation, made of calcium silicate, was 3 cm thick sideways and 9 cm upwards. On the sides of the array, the insulation plates were extended well below the fin boundaries, as shown in Fig. 4, so as to force a two-dimensional external free convection flow (i.e. with no sideway velocity component). Copper–constantan thermocouples were used for temperature measurements at various points of the fin array and insulation. In all the tests, the exposed fin array surface, of the base and fins, was found to be isothermal (owing to a small Biot number). To evaluate the convective heat transfer rate, radiative heat fluxes and heat losses through the insulation were, both, calculated and deducted from the input power. The radiative heat losses were evaluated based on a known shape factor and a network formula [6]. The surface emissivities were 0.87 and 0.95, since two different coatings were used. The experimental average heat transfer coefficient was simply obtained from the division of the convective heat transfer rate by, both, the total surface fin array area and the surface to ambient temperature difference. The error of the experimental heat transfer coefficient is smaller than 10% [7]. The test apparatus reliability was demonstrated through the successful reproduction of published experimental data on the heat transport underneath flat strips.

Table 1
Geometrical dimensions for the investigated cases

	Case					
	1	2	3	4	5	6
H [cm]	1.05	2.15	3.4	3.4	3.4	3.4
$2L$ [cm]	20	20	20	13	26	39
$2a$ [mm]	7	7	7	7	7	7
$2t$ [mm]	2.2	2.2	2.2	2.2	2.2	2.2

4. Numerical solution

A numerical solution was obtained with the Icepak CFD code [8]. In principle, the code solves the governing set of elliptic partial differential equations for conservation of mass, momentum and energy. The buoyancy forces representation is based on the Boussinesq approximation. The flow is, therefore, considered as essentially incompressible. The fluid properties are assumed constant and are evaluated at the average of the hot surface and the ambient fluid temperatures. The solution is for conditions of steady state laminar free convection.

An illustration of the boundaries used for the numerical simulation is presented in Fig. 5. The channel is located at the upper surface of the rectangular control volume. Owing to the comprehensive capability of the code to conduct conductive and convective heat transfer calculations, it suffices to require isothermal surface conditions only at the channel upper base surface. The temperature distribution within the channel walls is calculated by the code, and the results indeed confirmed the expected isothermal conditions. The size of the control volume was extended horizontally and vertically up to the point that they ceased to influence the calculated flow and temperature fields of the boundary layer. In particular, this applies to the dimensions "d" and "b" shown in the figure. The characteristic dimensions that were found as adequate are $d = 0.4L$ and $b = 2L$, which are not different from those found for the horizontal strip simulation [3]. Further extension of those dimensions does not entail any perceptible difference in the calculated heat transfer coefficient. The ambient two-dimensional circulatory flow enters and leaves the control volume around the open enclosure sides, which are

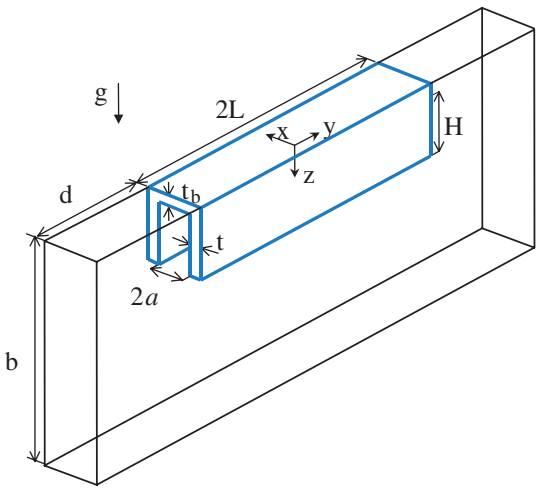

Fig. 5. Control volume for the numerical simulation of a hot finned surface.

$2(a+t)$ wide. At these open boundaries, according to the Icepak manual [8], viscosity effects are neglected and the pressure is assumed to be equal to the ambient pressure. Likewise, the flow entering the control volume is assumed to be at the ambient temperature. The other two control volume surfaces, at $x=\pm(a+t)$, are considered as surfaces of symmetry.

To solve the problem, the code divides the flow domain into control volumes. The numerical scheme integrates the governing equations over each control volume to construct a set of algebraic equations, after linearization of the results. The set is then solved iteratively by the Gauss–Seidel linear equation solver for algebraic multigrid systems (AMG) until convergence is achieved. For convergence determination, the dimensionless residual term of each equation was calculated after each iteration. Convergence was achieved when the residual terms of the continuity and momentum equations were smaller than 10^{-3}, and smaller than 10^{-7} for the energy equation. The computation results provided numerical velocity and temperature profiles from which heat transfer coefficients were calculated. Those results were successfully tested against current experimental data. They also accurately reproduced the velocity and temperature profiles of Aihara et al. [1] for the limiting case of a flat horizontal strip.

5. Results and discussion

The integration of the analytical solution requires a selection of adequate velocity and temperature profiles. Several choices were tested and the most successful was incorporated. The profiles must satisfy the boundary conditions. As such, two distinctly different regions exist in the boundary layer. One resides within the channels and the other outside the channels. Therefore two sets of profiles were selected and are

$$\frac{v}{v_{\max}}=\begin{cases}\frac{27}{4}\eta(1-\eta)^2(1-\xi^2), & 0\leqslant\eta\leqslant c\\ \frac{27}{4}\eta(1-\eta)^2, & c<\eta\leqslant 1\end{cases} \tag{19}$$

$$\frac{\theta}{\theta_{\mathrm{w}}}=\begin{cases}1-[1-(1-\eta)^n](1-\xi^2)m, & 0\leqslant\eta\leqslant c\\ \left\{1-\frac{2}{3}m[1-(1-c)^n]\right\}\left(\frac{1-\eta}{1-c}\right)^2, & c<\eta\leqslant 1\end{cases} \tag{20}$$

where

$$n=\frac{1}{4}+\frac{7}{4}\exp\left(-0.5\frac{H}{a}\right) \tag{21}$$

$$m=1+\frac{1}{2}\exp\left(-0.05\frac{H}{a}\right) \tag{22}$$

Substitution of these profiles into the analytical model and the subsequent integration constitute a lengthy and quite cumbersome process. Nevertheless, it provides all the components of the analytical solution, Eq. (15). The solution, though complex, predicts quite accurately, both, the experimental results and the numerical simulation. However, exploration of its terms revealed that it can be substantially simplified by substitution of some of its complex functions (such as the hyper-geometric function) by simple form approximations. The substitutions made for $Pr=0.7$, yield the following approximation

$$\frac{f_7}{2}C_1^{-\frac{1}{5}}F\left(\frac{1}{5},\frac{1}{2};\frac{3}{2};\frac{C_2}{C_1}\right)(Ra_LPr)^{\frac{1}{5}}+\frac{f_{10}}{c}\left(\frac{H}{a}\right)\left(\frac{L}{a}\right)\approx 0.46\exp\left(-\frac{H}{2a}\right)Ra_L^{\frac{1}{5}}+0.3\left(\frac{H}{a}\right)\left(\frac{L}{a}\right)^{-\frac{4}{5}}Ra_L^{\frac{2}{5}} \tag{23}$$

The solution must reduce to that of the horizontal infinite flat strip when the fin height approaches zero. Furthermore, to make it also compatible with the limiting case of short strips, it is necessary to multiply the solution by the term in squared parenthesis of Eq. (2). This term accounts for the influence of the "edge effects" on the heat convection of short flow paths, when they are of significance. The adoption of this correction and its introduction into channel correlations turned out to be warranted. With the substitution of Eq. (23) and the incorporation of the "edge effects" correction, the averaged Nusselt number takes the form of

$$\overline{Nu}_L=\frac{\overline{Nu}_L^{\infty}}{1+\frac{H}{a}}\left[\exp\left(-\frac{H}{2a}\right)+0.65\left(\frac{H}{a}\right)\left(\frac{L}{a}\right)^{-\frac{4}{5}}Ra_L^{\frac{1}{5}}\right] \tag{24}$$

where $\overline{Nu}_L^{\infty}$ is the averaged Nusselt number for the horizontal infinite flat strip, presented by Eq. (2). Notice that this correlation is a simple, self-contained, closed form solution.

The comparison of the analytical, numerical and experimental results for six different fin arrays (listed in Table 1) is presented in Fig. 6. As seen, the numerical and test data are in an exceptional agreement. Likewise, the analytical model predicts reasonably well the test results. Excluding the 13 cm array (6.5 cm flow path length), the deviations of the predicted heat transfer coefficients from, either, the numerical or experimental results are smaller than 5%. The shortest array, represents an extreme case were the longitudinal flow path is 6.5 cm and the fin height is 3.4 cm. For that case, the maximum deviation is smaller than 12% and is reached only at the higher temperatures. It is worth noting that without the edge effect correction, that deviation would have been larger. Notice also that at low temperatures, the deviation vanishes.

As expected, owing to stronger buoyant forces, the heat transfer coefficient always increases with the array surface temperature. Inspection of the influence of the fin height on the averaged heat transfer coefficient

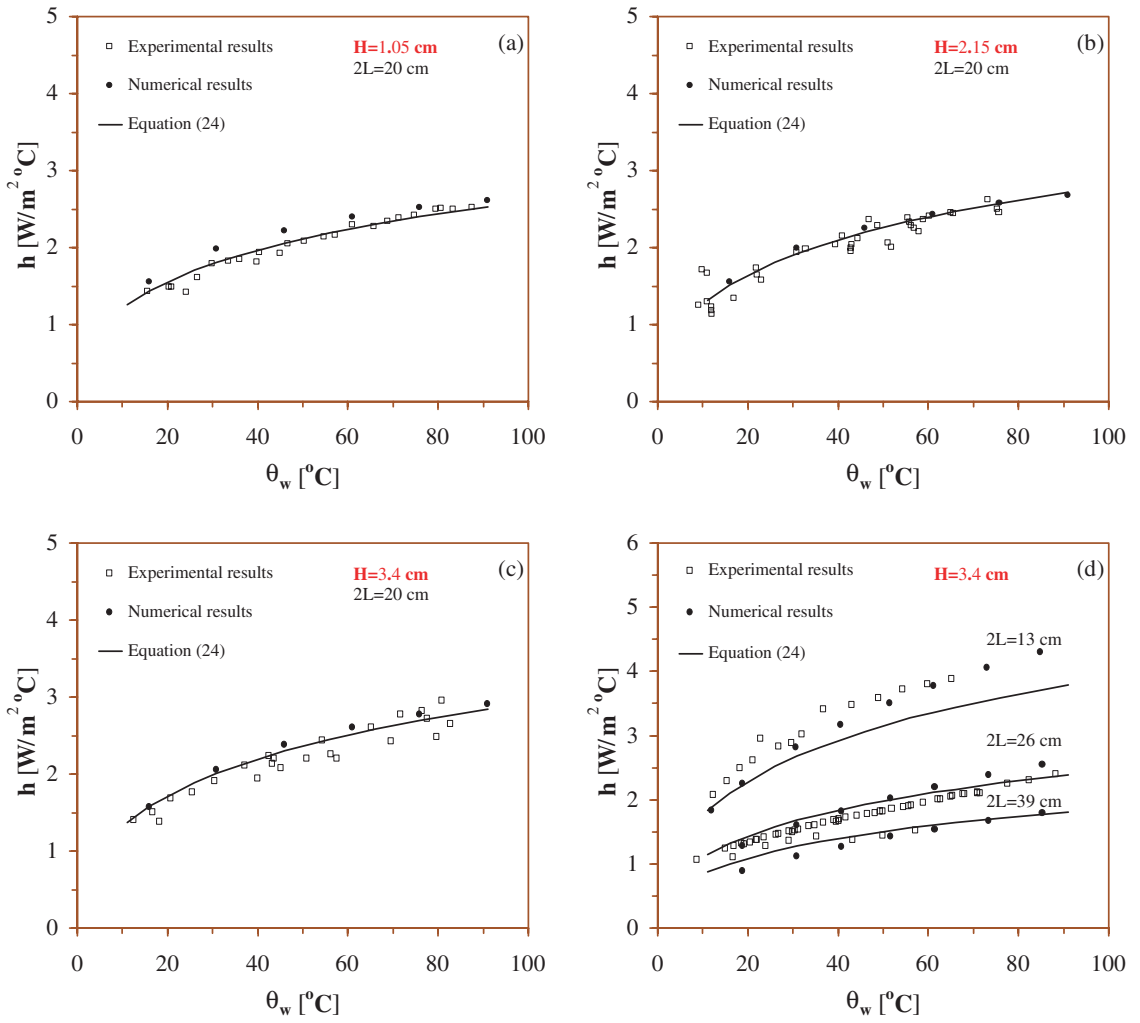

Fig. 6. The dependence of the heat transfer coefficient on the temperature difference for various array geometries. (a)–(c) Effect of fin height; (d) effect of array length.

indicates that it is quite small. As opposed to that, the influence of the channel length is substantial. To further demonstrate those sensitivities, the dependence of the heat transfer coefficient on, both, the fin height and channel length is plotted in Fig. 7, for two different array surface temperatures. It is seen that at certain fin heights the heat transfer coefficient has a minimum. This stems from the fact that up to a certain height the increase of the fin heights does not enhance the buoyant force but increases the drag force, and thus reduces the averaged heat transfer coefficient. Beyond that height, there is a mutual compensation between the two effects with a slightly stronger influence of the buoyant force, since it is after all the flow driver. Note that the above discussion is for the average heat transfer per unit surface area. However, any increase of fin height increases the array surface area and thereby entails a larger heat transfer rate. The influence of the channel length is obviously one of increased resistance to the flow at longer channels, and thus of smaller heat transfer coefficients. Experimental data are also shown in Fig. 7 as well as points representing the flat-strip heat transfer coefficients, calculated numerically. The agreement between the theoretical predictions and all the other data, including numerical, is excellent.

The fin spacing plays an important role in determining the array heat transport capability. As seen in Fig. 8, larger fin spacing in effect reduces drag and thereby increases the heat transfer coefficient. However, for specified array base dimensions, enlargement of the fin spacing reduces the cooling surface area. The opposing influence of these two effects on the heat

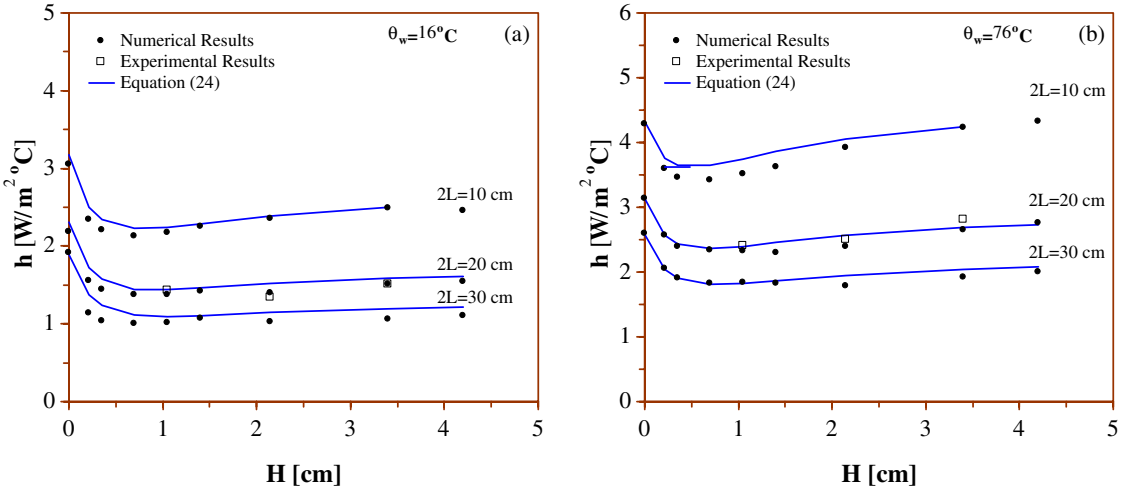

Fig. 7. The dependence of the heat transfer coefficient on the fin height for various array lengths ($2a = 7$ mm): (a) at $\theta_w = 16$ °C; (b) at $\theta_w = 76$ °C.

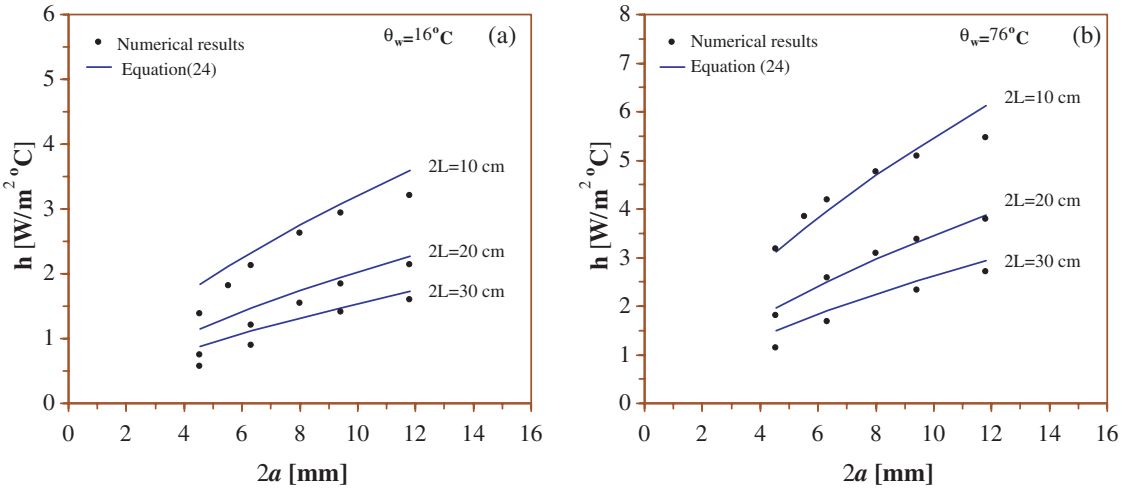

Fig. 8. The dependence of the heat transfer coefficient on the fin spacing for various array lengths ($H = 3.4$ cm): (a) at $\theta_w = 16$ °C; (b) at $\theta_w = 76$ °C.

transfer rate per unit base area is illustrated in Fig. 9 (computed numerically). It is seen that they entail optimal fin spacing. On each curve, the optimum was marked with a dot. Clearly, the optimal spacing is independent of the fin height, since the latter does not affect much the heat transfer coefficient above a certain height (see Fig. 7). The importance of the fin height is in the added cooling area that it can provide, as seen in Fig. 9a.

The influence of the array surface emissivity on the optimal fin spacing is also negligible, as shown in Fig. 9b (radiation calculations, as previously mentioned, were based on [6]). In free convection problems, thermal radiation can play an important role in the total fin array cooling capacity. Furthermore, radiation has its own optimal spacing. However, this optimum is pronounced only when the surface emissivity is small. At this instance, the relative importance of radiation is fairly small and therefore is non-influential. When the radiation becomes strong, owing to large surface emissivity, the fin spacing weakly affects the radiation component.

The array surface temperature has a small effect on the optimal fin spacing, as seen in Fig. 9c. This is

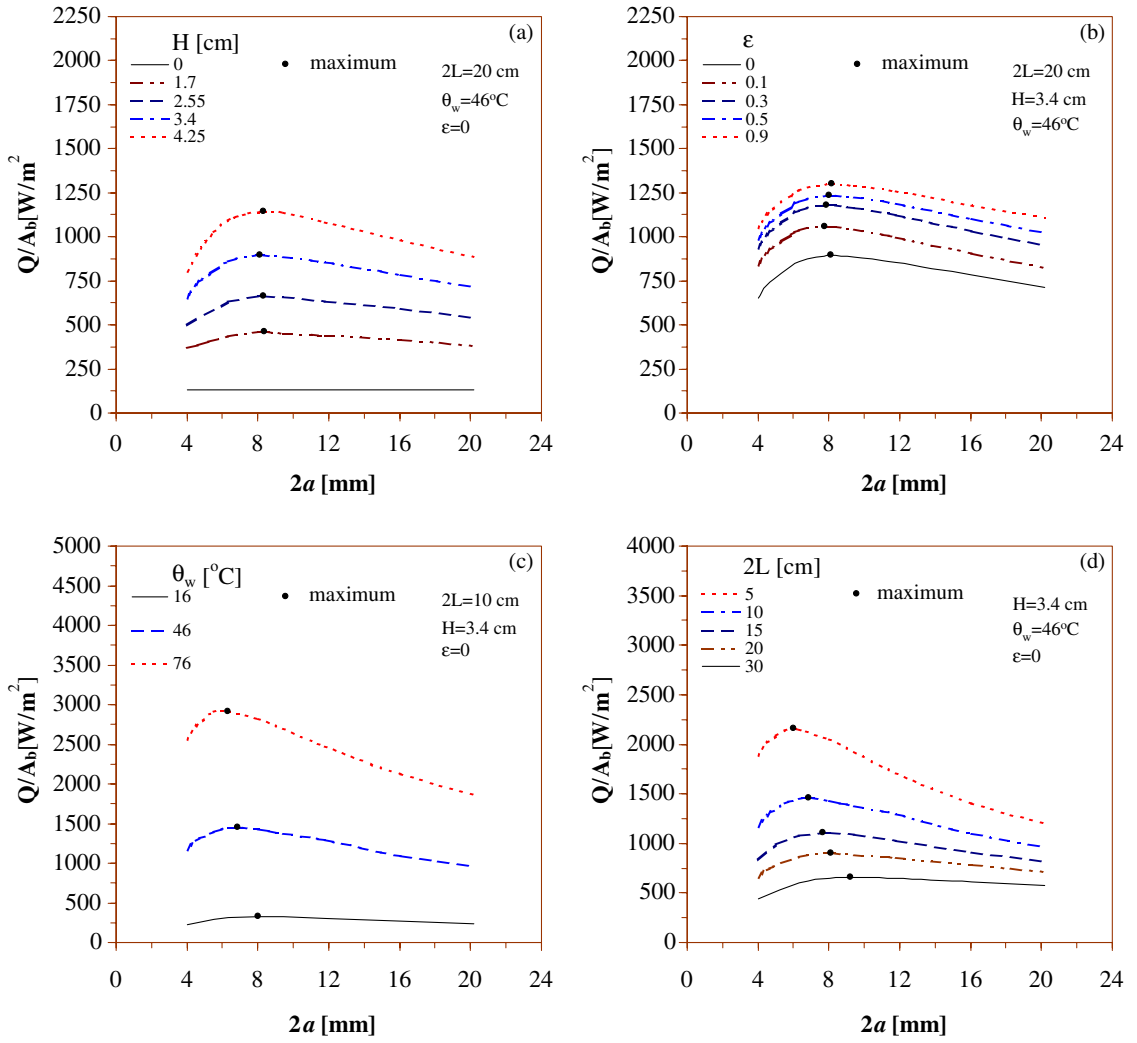

Fig. 9. Effects of fin spacing on the heat transfer rate per array unit base area, for different fin heights (a), surface emissivities (b), surface temperatures (c), and array length (d).

attributed to the fact that with higher temperature, buoyancy can still drive an effective convective flow into the tighter channels.

As depicted in Fig. 9d, the channel length has an appreciable influence on the optimal fin spacing. A long channel presents considerable flow resistance and therefore should be compensated by larger fin spacing. Another important feature revealed by the figure is that shorter channels are always preferable over longer ones. It indicates that the fin must be installed on a rectangular array in parallel to its short side. The most striking outcome of the above investigation it that the optimal fin spacing lies in a very narrow range for a wide variety of array geometries, from which the channel length is the one of real relevance.

The above discussion on the optimal spacing can considered as an optimization analysis that reveals what is the minimum fin height that can provide a specified cooling capacity for a given base area. The array base width (that equals the channel length $2L$) essentially determines the optimal fin spacing. Subsequently, the minimum fin height that provides enough cooling capacity is determined.

6. Conclusions

A combined analytical, numerical and experimental investigation of the free convection underneath a horizontal hot fin array was conducted. A useful closed form

correlation for the Nusselt number was developed for the first time. Furthermore, by accounting for both heat conduction and thermal radiation, it was possible to determine the optimal fin spacing that maximizes the heat transfer rate per unit of array base area for a given fin height. The following conclusions were drawn from that investigation:

- The integral method can be applied successfully to obtain closed form solutions for geometries where the existence of similarity profiles is somewhat dubious.
- The fin geometry can be slightly altered to facilitate analytical analyses without appreciable loss of accuracy.
- The array length, fin spacing, and surface temperature mostly affect the heat transfer coefficient. The fin height does not affect much the heat transfer coefficient.
- An optimal fin spacing exists which can be determined simply from the knowledge of the fin array length.

Excellent agreement was obtained among the analytical, numerical and experimental results.

Appendix A

The boundary layer thickness at the channel edge, δ_C, is calculated for critical flow conditions at that point. Over half of the channel width, the conducted energy transfer into the channel, $Q/2$, must be convected out of the channel edge. This energy is calculated by integrating the total enthalpy across the channel at the edge. The integration is based on the velocity and temperature profiles of Eq. (5), subject to a variable air density in the buoyancy and pressure terms. The pressure is calculated according to Eq. (3d) for a reference value P_{ref} at a distance z_{ref} below the channel (see Fig. 10). The integration of the total enthalpy at the channel edge is therefore

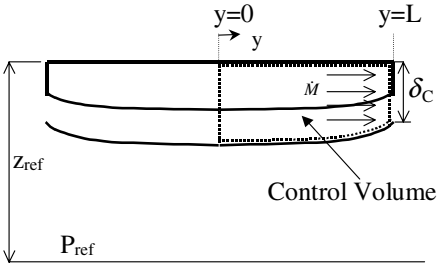

Fig. 10. Boundary layer schematics for the calculation of the critical depth.

$$
\begin{aligned}
Q/2 &= \int_{-a}^{a}\int_{0}^{\delta_C}\left[\left(\mathbf{u}+\frac{v^2}{2}-gz+\frac{p}{\rho}\right)\rho v\right]_{|y=L}\mathrm{d}z\,\mathrm{d}x \\
&= \dot{U} + f_8\rho_\infty v^3_{\max(L)}\delta_C a + f_9\rho_\infty g\beta\theta_w\delta_C^2 v_{\max(L)}a \\
&\quad + f_0 P_{ref} v_{\max(L)}\delta_C a - f_0\rho_\infty g z_{ref}\delta_C v_{\max(L)}a
\end{aligned}
\tag{A.1}
$$

where $\mathbf{u}$ and $\dot{U}$ represent the fluid specific internal energy and its flux at the channel edge, respectively and

$$
f_8 = \frac{1}{2}\int_{-1}^{1}\int_{0}^{1} v^{*3}\,\mathrm{d}\eta\,\mathrm{d}\xi
$$

$$
f_9 = \int_{-1}^{1}\int_{0}^{1}\left[\left(\int_{\eta}^{1}\theta^*\,\mathrm{d}\eta'\right)v^* + \theta^* v^*\eta\right]\mathrm{d}\eta\,\mathrm{d}\xi
$$

$$
f_0 = \int_{-1}^{1}\int_{0}^{1} v^*\,\mathrm{d}\eta\,\mathrm{d}\xi
$$

The mass discharge rate at the channel edge is

$$
\dot{M} = \int_{-a}^{a}\int_{0}^{\delta_C}(\rho v)_{|y=L}\,\mathrm{d}z\,\mathrm{d}x = f_0\rho_\infty v_{\max(L)}\delta_C a \tag{A.2}
$$

Combining Eqs. (A.1) and (A.2), to identify $\dot{M}$, yields

$$
\dot{U} + \frac{f_8\dot{M}^3}{f_0^3\rho_\infty^2\delta_C^2 a^2} + \frac{f_9 g\beta\theta_w\delta_C\dot{M}}{f_0} + \frac{p_{ref}\dot{M}}{\rho_\infty} - gz_{ref}\dot{M} - \frac{Q}{2} = 0 \tag{A.3}
$$

Equating the derivative of Eq. (A.3) to zero enables the calculation of the maximum discharge rate $\dot{M}$ for an energy input $Q/2$. This is done according to

$$
\frac{\mathrm{d}\dot{M}}{\mathrm{d}\delta_C} = 0 \tag{A.4}
$$

Since most of the convected energy $Q/2$ is in the thermal component $\dot{U}$, it is assumed that the derivative of their difference $(Q/2-\dot{U})$ with respect to δ_C is negligible. It implies that conditions of critical flow are dictated by how the mechanical energy redistributes itself among the pressure, the kinetic and the potential components at the point of discharge. With this assumption, the critical flow was found to be

$$
\delta_C^3 = \frac{2f_8\dot{M}^2}{f_9 f_0^2 g\beta\theta_w\rho_\infty^2 a^2} \tag{A.5}
$$

Substitution of Eq. (A.2) yields

$$
\delta_C = \left(\frac{2f_8 f_{33}^2\alpha^2 L^2}{f_9 g\beta\theta_w}\right)^{1/5} \tag{A.6}
$$

References

[1] T. Aihara, Y. Yamada, S. Endo, Free convection along the downward facing surface of a heated horizontal plate, Int. J. Heat Mass Transfer 15 (1972) 2535–2549.

[2] T. Fujii, H. Imura, Natural-convection heat transfer from a plate with arbitrary inclination, Int. J. Heat Mass Transfer 15 (1972) 755–767.
[3] A. Dayan, R. Kushnir, A. Ullmann, Laminar free convection underneath a hot horizontal infinite flat strip, Int. J. Heat Mass Transfer 45 (2002) 4021–4031.
[4] R.L. Daugherty, J.B. Franzini, Fluid Mechanics with Engineering Applications, seventh ed., McGraw Hill, 1977, pp. 334–337.
[5] M. Sadatom, M. Kawaji, C.M. Lorencez, T. Chang, Prediction of liquid level distribution in horizontal gas–liquid stratified flows with interfacial level gradient, Int. J. Multiphase Flow 19 (6) (1993) 987–997.
[6] B. Abramzon, A simple closed-form solution for evaluation of radiative heat transfer from a rectangular fin array, IEEE Trans. Components, Packag. Manuf. Technol.—Part A 20 (2) (1997) 225–229.
[7] G. Mittelman, Experimental study of free convection from a hot finned surface facing down, M.Sc., Tel Aviv University, Ramat Aviv, 2001.
[8] Fluent Inc., Icepak 3 User's Guide, 1999.